1990ApJ...364..212H

THE ASTROPHYSICAL JOURNAL, 364:212–221, 1990 November 20
© 1990. The American Astronomical Society. All rights reserved. Printed in U.S.A.

LUMINOSITY PROFILES AND THE EVOLUTION OF SHOCK WAVES IN GENERAL-RELATIVISTIC RADIATING SPHERES

L. HERRERA
Departamento de Física, Facultad de Ciencias, Universidad Central de Venezuela

AND

L. A. NÚÑEZ
Laboratorio de Física Teórica, Departamento de Física, Facultad de Ciencias, Universidad de Los Andes, and International Centre for Theoretical Physics, Trieste-Italy
Received 1989 March 23; accepted 1990 May 1

ABSTRACT

A method recently proposed by the authors to study the evolution of discontinuities in radiating spherically symmetric distributions of matter is systematically applied to model the evolution of a composite radiant sphere. The matter configuration, free of singularities, is divided in two regions by a shock wave front, and at each side of this interface a different equation of state is considered. Solutions are matched across the shock via the Rankine-Hugoniot conditions, while the outer region metric joins the Vaidya solution at the boundary surface. The influence on the evolution of these composite spheres of different shapes of neutrino outburst profiles and particular neutrino-transfer processes from the inner core to the outer mantle is explored. Prospective applications to supernova scenarios are discussed.

Subject headings: neutrinos — shock waves — stars: supernovae

I. INTRODUCTION

The discovery of the supernova SN 1987A and the observation of its associated neutrino pulse have renewed the interest in the problem of gravitational collapse of massive stars ($M_* > 8\ M_\odot$). For the first time, a recorded neutrino profile provides a wealth of observational and experimental data about the nature of the processes producing the final compact remnant. However, interesting controversies have been raised over both the form of the detected neutrino outburst profile and the possible hydrodynamic scenarios compatible with this detection. The discrepancies between the data collected by Kamiokande II (Hirata *et al.* 1987) and Irvine-Michigan-Brookhaven (IMB) (Bionta *et al.* 1987) groups and those reported by the Mont Blanc detector (Aglietta *et al.* 1987) have motivated a fruitful debate over the specific contour that might represent the detected burst (De Rújula 1987). The hydrodynamic pictures proposed to be consistent with this first observation range from the prompt Type II supernova (Baron *et al.* 1987; Bruenn 1987; Kahana, Cooperstein, and Baron 1985) and the advective overturn detonation mechanism (Arnett 1987) to the two-bang explosion yielding either a black hole (Aglietta *et al.* 1987; Hillebrandt *et al.* 1987), a neutron star (De Rújula 1987), or disruption of a light neutron star in a ultra–close binary system (Stella and Treves 1987). The diversity of proposed explanations has stimulated reworking of the neutrino physics involved in order to establish a definite conclusion about the detailed aspects of the interior current supernova processes from the observed data (Sawyer 1988; Lattimer 1988). Besides the decisive roles played by the neutrinos on the supernovae outcome, it is a well-established fact that during the implosion the core pulls away from the rest of the star and the flow is separated into an inner subsonic core and an outer supersonic mantle by a discontinuity surface (a shock).

In this context, it is interesting to explore the influence that different pulse signatures would have on the hydrodynamics of a radiating general-relativistic composite sphere. We have proposed in recent work (Herrera and Núñez 1987) a method to study the evolution of a general-relativistic radiating fluid sphere divided in two regions by a shock wave front. At either side of the shock wave front, a physically reasonable equation of state is chosen. In the static limit the inner region corresponds to the homogeneous Schwarzschild incompressible fluid, whereas the outer mantle represents a highly compressed Fermi gas. The solutions corresponding to either side of the front are matched across it via the Rankine-Hugoniot conditions (Taub 1948, 1983; Herrera and Núñez 1987). Matching with the Vaidya metric on the boundary of the configuration completes the consistency of this radiating sphere. A heuristic assumption relating pressure, energy density, and the radial velocity of matter is introduced. This *Ansatz*, together with the junction conditions at the shock and at the boundary of the matter distribution, leads to a system of ordinary differential equations for quantities evaluated at either the boundary surface or the shock front. The numerical integration of this system allows us, using the field equations, to find the profile of the physical variables throughout. The luminosity has been assumed to be a Gaussian-like pulse which carries out a fraction of the total initial mass.

The present paper illustrates a systematic application of the method. It is apparent from the modeling performed that the outer matter shells bounce earlier than inner ones. This very peculiar scenario seems to be closely related to the specific regime of radiation transport assumed (free streaming out) for the Tolman VI–like equation of the outer mantle. We shall comment further on this point in the last section. It is important to keep in mind that, in the context of the present approach, the shock wave is to be considered as an interface separating the quasi-static stiff core from the outer mantle. In all the models presented below, this interface fades out and becomes a new boundary surface delimiting the compact homogeneous remnant.

In the present work, we are particularly interested in simulating departures, at the interface and at the boundary surface, from the streaming-out limit approximation for the radiation field. This is carried out in two ways: (*a*) by modifying the contour of the

© American Astronomical Society • Provided by the NASA Astrophysics Data System

1990ApJ...364..212H

radiation flux emission at the boundary of the configuration and at each side of the shock wave front; and (*b*) by introducing "time delays" between absorption and emission of the radiation flux pulse at the interface and on the boundary surface.

This paper is organized as follows. In § II, the conventions used in this paper, the Einstein field equations, and a brief outline of the method are sketched. Section III contains a description of the models worked out. The discussion of the results is presented in § IV. The Appendix resumes an erratum in Herrera and Núñez (1987).

II. FIELD EQUATIONS AND THE METHOD

For completeness we outline here the method presented in our previous paper (Herrera and Núñez 1987). Let us consider a nonstatic distribution of matter which is spherically symmetric. In radiation coordinates (Bondi 1964) the metric takes the form

$$ds^2 = e^{2\beta}[(V/r)du^2 + 2\,du\,dr] - r^2(d\vartheta^2 + \sin^2\vartheta\,d\varphi^2)\,, \tag{1}$$

where β and V are functions of u and r. Here $u = x^0$ is the timelike coordinate, $r = x^1$ is the null coordinate, and $\vartheta = x^2$ and $\varphi = x^3$ are the usual angle coordinates. The u-coordinate is the retarded time in flat spacetime, and therefore u-constant surfaces are null cones open to the future. This last fact can be readily noticed from the relationship between these coordinates and the usual *Schwarzschild coordinates* (T, R, Θ, Φ):

$$\begin{aligned} u &= T - \int \frac{r}{V}\,dr\,, \qquad & \vartheta &= \Theta\,, \\ r &= R\,, & \varphi &= \Phi\,. \end{aligned} \tag{2}$$

The hydrodynamic scenario, as viewed by a local Minkowskian observer comoving with the fluid, consists of

1. An isotropic fluid of density $\hat{\rho}$ and pressure $\hat{P}$;
2. Isotropic radiation energy density $3\mathscr{P}$;
3. Unpolarized radiation energy density $\hat{\epsilon}$ traveling in the radial direction.

The energy momentum tensor describing this fluid can be written as (Bondi 1964; Herrera, Jiménez, and Ruggeri 1980)

$$\mathbf{T}_{\mu\nu} = (\rho + P)U_\mu U_\nu - Pg_{\mu\nu} + \epsilon K_\mu K_\nu\,, \tag{3}$$

where $\rho = \hat{\rho} + 3\mathscr{P}$, $P = \hat{P} + \mathscr{P}$, and the flux of radiation $\hat{\epsilon}$, as measured by the local Minkowski observer, is related to ϵ by

$$\epsilon = \hat{\epsilon}\,\frac{1+\omega}{1-\omega}\,. \tag{4}$$

The four-velocity vector U_μ and the null vector K_μ can be written as

$$U_\mu = \delta_\mu{}^0 e^{\beta}(1-\omega^2)^{-1/2}\left(\frac{V}{r}\right)^{1/2} + \delta_\mu{}^1 e^{\beta}\left(\frac{V}{r}\right)^{-1/2}\left(\frac{1-\omega}{1+\omega}\right)^{1/2}\,, \tag{5}$$

and

$$K_\mu = \delta_\mu{}^0 e^{\beta}\left(\frac{V}{r}\right)^{1/2}\,. \tag{6}$$

Using equations (1), (3), (5), and (6) the Einstein equations can be expressed as (Bondi 1964; Herrera, Jiménez, and Ruggeri 1980):

$$\frac{\rho + P\omega}{1-\omega^2} + \epsilon = \frac{1}{4\pi r(r-2\tilde{m})}\left(-\tilde{m}_0\,e^{-2\beta} + 1 - \frac{2\tilde{m}}{r}\right)\,, \tag{7a}$$

$$\frac{\rho + P\omega}{1-\omega^2} = \frac{\tilde{m}_1}{4\pi r^2}\,, \tag{7b}$$

$$\frac{1-\omega}{1+\omega}(\rho + P) = \frac{r-2\tilde{m}}{2\pi r^2}\beta_1\,, \tag{7c}$$

$$P = \frac{-\beta_{01}e^{-2\beta}}{4\pi} + \frac{1}{8\pi}\left(1 - \frac{2\tilde{m}}{r}\right)\left(2\beta_{11} + 4\beta_1^2 - \frac{\beta_1}{r}\right) + \frac{3\beta_1(1-2\tilde{m}_1) - \tilde{m}_{11}}{8\pi r}\,. \tag{7d}$$

We have denoted differentiation with respect to u and r by the suffixes 0 and 1, respectively, and have used

$$V = e^{2\beta}[r - 2\tilde{m}(u, r)]\,. \tag{8}$$

The matter radial velocity ω measured by a local Minkowski is related to the velocity of matter in the radiative coordinates by

$$\frac{dr}{du} = \frac{V}{r}\,\frac{\omega}{1-\omega}\,. \tag{9}$$

© American Astronomical Society • Provided by the NASA Astrophysics Data System

1990ApJ...364..212H

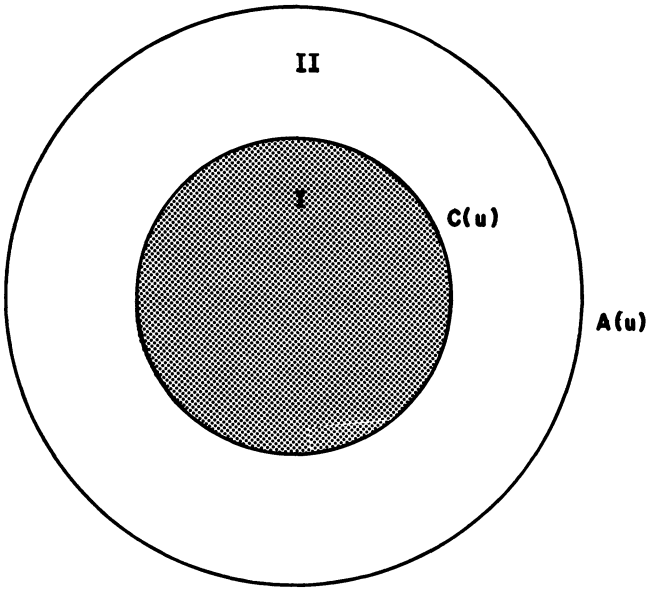

FIG. 1.—The two-region model sphere considered throughout this work. Region I, the inner core, is enclosed by a shock surface $C(u)$. The outer mantle completes the sphere of radius $A(u)$.

The field equations may be integrated outside the matter configuration to obtain

$$\beta = 0\,, \qquad V = r - 2m(u)\,, \qquad \epsilon = \frac{-m_0}{4\pi r(r-2m)}\,, \tag{10}$$

where m is a function of integration depending on u. Inside, the function $m(u)$ is generalized to $\tilde{m}(u, r)$ everywhere within the matter configuration.

It is sufficient to provide β and $\tilde{m}$ to calculate the physical variables ρ, P, ω, and ϵ algebraically from equations (7a)–(7d). Let us now define two auxiliary functions to accomplish this task. They will be hereafter referred to as the effective density and the effective pressure, respectively:

$$\tilde{\rho} = \frac{\rho - P\omega}{1+\omega}\,, \tag{11a}$$

$$\tilde{P} = \frac{P - \rho\omega}{1+\omega}\,, \tag{11b}$$

Observe that field equations (7b) and (7c) can be integrated:

$$\tilde{m} = \int_{a(u)}^{r} 4\pi r^2 \tilde{\rho}\, dr\,, \tag{12a}$$

$$\beta = \int_{a(u)}^{r} \frac{2\pi r^2}{r - 2\tilde{m}} (\tilde{\rho} + \tilde{P}) dr\,, \tag{12b}$$

where $r = a(u)$ defines the boundary of the fluid sphere.

The composite sphere of radius $a(u)$ is divided in two regions, called I and II, by a discontinuity surface (a shock) of radius $c(u)$ (see Fig. 1). Both $a(u)$ and $c(u)$ are functions of the timelike coordinate.

The matching conditions across the shock (the Rankine-Hugoniot conditions) require the continuity of the first and the second fundamental form plus

$$[T_{\mu\nu} n^{\nu}]_c = 0\,, \tag{13}$$

where $\mathbf{T}_{\mu\nu}$ is the energy-momentum tensor, n^{ν} is the unit vector normal to the surface $r = c(u)$ (Taub 1948, 1983), and

$$[f]_c = f|_{r=c+0} - f|_{r=c-0}\,.$$

These junction conditions at $r = c(u)$ lead to (see Herrera and Núñez 1987)

$$(1 - \Psi)[\tilde{\rho}]_c = \Psi[\tilde{P}]_c\,, \tag{14a}$$

and

$$[\Omega_s(\Omega_s - 1)(\tilde{\rho} + \tilde{P}) + (1 - \Psi)\tilde{\rho} + \epsilon]_c = 0\,, \tag{14b}$$

© American Astronomical Society • Provided by the NASA Astrophysics Data System

1990ApJ...364..212H

where

$$\Omega_s = \left(\frac{1}{1-\omega}\right)_{c\mp 0}, \qquad s = \mathrm{I}, \mathrm{II},$$

and

$$\Psi = 1 + \dot{c}e^{-2\beta}\left(1 + \frac{2\tilde{m}}{r}\right)^{-1}. \tag{15}$$

Using the field equations (7b) and (7c), we obtain for the metric functions β and $\tilde{m}$

$$\tilde{m}_{\mathrm{I}} = \int_0^r 4\pi r^2 \tilde{\rho}_{\mathrm{I}}\, dr, \qquad 0 \le r \le c(u); \tag{16a}$$

$$\tilde{m}_{\mathrm{II}} = \int_{c(u)}^r 4\pi r^2 \tilde{\rho}_{\mathrm{II}}\, dr + \tilde{m}_{\mathrm{I}}[u, c(u)], \qquad c(u) \le r \le a(u); \tag{16b}$$

and

$$\beta_{\mathrm{I}} = \int_{c(u)}^r \frac{2\pi r^2}{r - 2\tilde{m}_{\mathrm{I}}}(\tilde{\rho}_{\mathrm{I}} + \tilde{P}_{\mathrm{I}})dr + \beta_{\mathrm{II}}[u, c(u)], \qquad 0 \le r \le c(u); \tag{17a}$$

$$\beta_{\mathrm{II}} = \int_{a(u)}^r \frac{2\pi r^2}{r - 2\tilde{m}_{\mathrm{II}}}(\tilde{\rho}_{\mathrm{II}} + \tilde{P}_{\mathrm{II}})dr, \qquad 0 \le r \le c(u); \tag{17b}$$

where the subscripts I and II indicate the region the quantity is referred to. We can restate the algorithm for the composite sphere as follows:

1. Take two static interior solutions of the Einstein equations for fluids with spherical symmetry,

$$\rho_{\mathrm{st\,I}} = \rho_{\mathrm{I}}(r), \qquad \rho_{\mathrm{st\,II}} = \rho_{\mathrm{II}}(r);$$
$$P_{\mathrm{st\,I}} = P_{\mathrm{I}}(r), \qquad P_{\mathrm{st\,II}} = P_{\mathrm{II}}(r).$$

2. Assume that the r dependence of $\tilde{P}_{\mathrm{I,II}}$ and $\tilde{\rho}_{\mathrm{I,II}}$ is the same as that of $P_{\mathrm{st\,I,II}}$ and $\rho_{\mathrm{st\,I,II}}$, but considering the boundary condition which, for this case, reads

$$\tilde{P}_{\mathrm{II}a} = -\omega_a \tilde{\rho}_{\mathrm{II}a},$$

with the conditions at $r = c(u)$ given by equations (14a) and (14b).

3. Given the r dependence of $\tilde{\rho}_{\mathrm{I,II}}$ and $\tilde{P}_{\mathrm{I,II}}$ and using equations (16a)–(17b), we get $\tilde{m}_{\mathrm{I,II}}$ and $\beta_{\mathrm{I,II}}$ up to some functions of u which will be specified below.

4. For these functions of u we obtain the following ordinary differential equations (surface equations). Three of them (two are model-independent) emerge because of the junction conditions and the field equations evaluated at the boundary surface. The remainder of the surface equations comes from the Rankine-Hugoniot conditions (14a) and (14b).

a) The first surface equation comes from the definition (9) evaluated at the boundary $r = a(u)$, which, after scaling the radius a, the total mass m, and the timelike coordinate u by the initial mass $m(u = 0) = m(0)$,

$$A = a/m(0), \qquad M = m/m(0), \qquad u/m(0) \Rightarrow u,$$

and defining

$$F = 1 - \frac{2M}{A}, \qquad \Omega = \frac{1}{1-\omega_a},$$

can be written as

$$\dot{A} = F(\Omega - 1). \tag{18}$$

b) The second surface equation relates the total mass-loss rate with the energy flux through the surface. This can be obtained by evaluating equation (7a) for $r = a + 0$ and takes the form

$$\dot{M} = -FE, \tag{19}$$

where the total luminosity E is defined by

$$E = (4\pi r^2 \epsilon)_{r=a(u)}.$$

Using the above definitions and equation (18), we can rewrite equation (19) as

$$\frac{\dot{F}}{F} = \frac{2E + (1-F)(\Omega - 1)}{A}. \tag{20}$$

© American Astronomical Society • Provided by the NASA Astrophysics Data System

1990ApJ...364..212H

c) The third equation at the surface is obtained from the conservation equation $T^{\mu}{}_{1;\mu} = 0$ evaluated at the surface. From

$$(T^{\mu}{}_{1;\mu})_a = 0 ,$$

we get

$$\left[\frac{(\tilde{\rho}+\tilde{P})}{(1-2\tilde{m}/r)}\right]_{,0a} - \left(\frac{\partial \tilde{P}}{\partial r}\right)_a - \left[\frac{(\tilde{\rho}+\tilde{P})}{(1-2\tilde{m}/r)}\left(4\pi\tilde{P}+\frac{\tilde{m}}{r^2}\right)\right]_a = 0 . \tag{21}$$

Notice that equations (18) and (20) are model-independent, while equation (21) should be particularly shaped for every model considered.

d) The remaining equations are also model-dependent and are written as a result of the matching conditions across $r = c(u)$.

5. Providing three additional functions, one evaluated at $r = a(u)$ and the other two evaluated at $r = c(u)$, the system (18), (20), (21) and the matching conditions may be integrated for any particular set of initial data.

6. By substituting the result of the integration in the expressions for $\tilde{m}_{\rm I,II}$ and $\beta_{\rm I,II}$, these four functions become completely determined.

7. By using equations (7a)–(7d), the matter variables ρ, P, ω, and ϵ may be found for any part of the sphere.

Finally, we sketch the assumptions for the effective variables. For the inner region a solution having as its static limit the well-known Schwarzschild homogeneous interior solution has been considered:

$$\tilde{\rho}_{\rm I} = f(u) , \tag{22}$$

and

$$\tilde{P}_{\rm I} = f(u)\left\{g(u)\left[1-\frac{8\pi}{3}r^2 f(u)\right]^{1/2} - \frac{1}{3}\right\}\Big/\left\{1-g(u)\left[1-\frac{8\pi}{3}r^2 f(u)\right]^{1/2}\right\} . \tag{23}$$

For the outer region the effective variables are chosen, inspired in the static Tolman VI metric (Tolman 1939):

$$\tilde{\rho}_{\rm II} = \frac{3h(u)}{r^2} , \tag{24}$$

$$\tilde{P}_{\rm II} = \frac{h(u)}{r^2}\left[\frac{1-9k(u)r}{1-k(u)r}\right] . \tag{25}$$

Functions $f(u)$, $g(u)$, $h(u)$, and $k(u)$ are arbitrary; however, $h(u)$ and $k(u)$ are related through the boundary condition $\tilde{P}_{\rm II} = -\omega_a \tilde{\rho}_{\rm II}$.

III. MODELING

The original incentive for the present work was to study the possible general-relativistic hydrodynamic scenarios associated to different forms of the received burst. However, the opportunity to shape the radiation profile at both sides of the shock motivates us additionally to simulate eventual complex neutrino-transfer phenomena, from the inner core to the outer mantle, enriching the corresponding hydrodynamic scenarios.

Modeling is performed, setting the initial data for the surface equations and the particular forms of the radiation flux energy density emission profiles at each side of the shock wave front and on the boundary surface. These emission contours have been selected to be shaped either by one or two consecutive Gaussian pulses characterized by the following parameters: (*a*) Pulse widths (variances) (PW1, PW2); (*b*) Time for the first peak (TFP); (*c*) Separation in time of the peaks (STP); (*d*) Pulse height ratio (PHR); (*e*) Total radiated energy (TRE). A standard model is defined as having

$$A\Big|_{u=0} = 20.000 , \qquad \Omega\Big|_{u=0} = 0.920 ,$$

$$F\Big|_{u=0} = 0.900 , \qquad C\Big|_{u=0} = 12.000 ,$$

$$G\Big|_{u=0} = 0.907 , \qquad D\Big|_{u=0} = -0.598 ,$$

as the set of initial data for the surface equation. It is worth mentioning that the surface equations are scale invariant in the sense that these initial data are given in terms of dimensionless (scaled) variables. The radiation profile is represented by one Gaussian pulse determined by

$$\mathrm{TFP} = 20.0 , \qquad \mathrm{PW1} = 1.2 .$$

The total radiated mass, at the surface and at both sides of the shock front, is expressed as a fraction of the total initial mass of the configuration. It is considered for the present calculations that 10^{-2} of the total initial mass is radiated at the boundary surface, and 10^{-5} is emitted at shock front.

The evolution of both the radius of the sphere (the boundary surface) and the shock wave front are sketched in Figure 2. Figures 3*a*–3*d* display the profiles for energy density, pressure, the radial velocity, and radiation flux density, respectively. The running time is suggested by the behavior of the matter variables themselves. They have been monitored at five different fixed-mass shells,

© American Astronomical Society • Provided by the NASA Astrophysics Data System

1990ApJ...364..212H

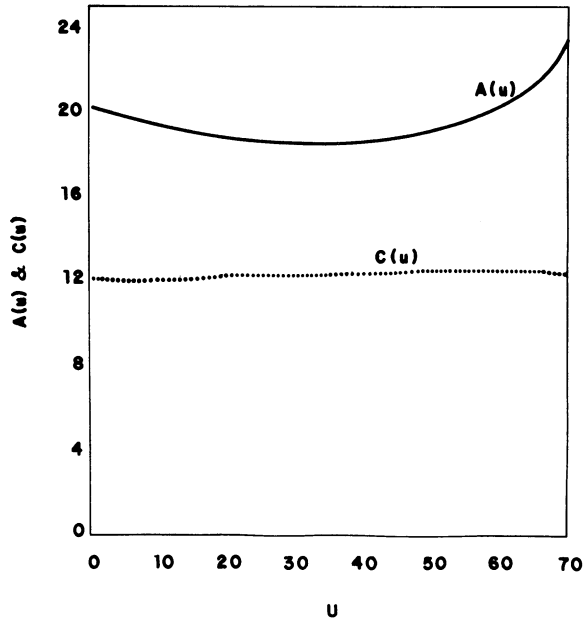

FIG. 2.—Time evolution of $A(u)$ and $C(u)$ for the standard exploding sphere

$r/a_0 = 0.2, 0.4, 0.6, 0.8$, and 1.0. Notice that these recordings have been made at fixed r/a_0 positions [except for $r/a_0 = 1.0$; a_0 is the initial value for the radius of the surface boundary: $a_0 = a(0)$], differing from the movable shells r/a of our previous work (Herrera and Núñez 1987). As is clear from equations (2), in these fixed shells the evolution of the physical variables, described from Bondi's coordinates (Bondi 1964), coincides with the description from the usual Schwarzschild's coordinates. Finally, Figure 4 represents the evolution of the shock intensity, defined as the pressure difference at both sides of the shock front $\mathcal{I} = P_{II} - P_I$.

In Table 1 we have resumed the influence of several factors over the mean shock intensity $\bar{\mathcal{I}}$ and over the strength of the bouncing. The numbers at the upper left corner on the squares placed at the first row and the first column label the different models sketched in the table. The standard model corresponds to the 00 position. Both the sign of the relative mean shock intensity

$$\text{SIGN}\,(\bar{\mathcal{I}}_{ij}) = \text{SIGN}\,(\bar{\mathcal{I}}_{ij} - \bar{\mathcal{I}}_{00})\,,$$

and the sign of the relative strength of the bouncing SIGN $(\mathcal{V}_{ij})$ of the other models are represented at the corresponding i, j address, where i indicates columns and j indicates rows. Radiant circles bigger than the one used for the standard model indicate stronger bounces, and smaller ones represent less violent rebounds.

The relative strengths of the bouncing has been defined as the quantity SIGN $(\mathcal{V}_{ij})$ as

$$\text{SIGN}\,\mathcal{V}_{ij} = \begin{cases} (+)\ \text{if} \begin{cases} \text{i)} & \text{SIGN}\,[A_{ij}(60) - A_{00}(60)] = (+)\,; \\ \text{ii)} & \begin{cases} \text{SIGN}\,[A_{ij}(60) - A_{00}(60)] = (0)\,, \\ \text{SIGN}\,[\dot{A}_{ij}(60) - \dot{A}_{00}(60)] = (+)\,; \end{cases} \end{cases} \text{and} \\ (-)\ \text{if} \begin{cases} \text{i)} & \text{SIGN}\,[A_{ij}(60) - A_{00}(60)] = (-)\,; \\ \text{ii)} & \begin{cases} \text{SIGN}\,[A_{ij}(60) - A_{00}(60)] = (0)\,, \\ \text{SIGN}\,[\dot{A}_{ij}(60) - \dot{A}_{00}(60)] = (-)\,; \end{cases} \end{cases} \text{and} \end{cases}$$

where $A(60) = A(u)|_{u=60}$, and $\dot{A}(60) = \dot{A}(u)|_{u=60}$, and we have associated

$$\text{more violent bouncing} \Leftrightarrow \text{SIGN}\,\mathcal{V}_{ij} = (+)\,,$$

$$\text{less violent bouncing} \Leftrightarrow \text{SIGN}\,\mathcal{V}_{ij} = (-)\,.$$

Symbols for the relative mean shock intensities are

$$|||\Rightarrow \quad \text{strong shocks} \quad \Rightarrow \text{SIGN}\,(\bar{\mathcal{I}}_{ij}) = (+)\,,$$

$$||\Rightarrow \quad \text{standard shock} \quad \Rightarrow \text{SIGN}\,(\bar{\mathcal{I}}_{ij}) = (0)\,,$$

$$|\Rightarrow \quad \text{weak shocks} \quad \Rightarrow \text{SIGN}\,(\bar{\mathcal{I}}_{ij}) = (-)\,.$$

On the squares at the first row (cols. [1]–[9]) the different modifications of the standard value of the total energy flux density at both sides of the shock (ϵ_I for region I, ϵ_{II} for region II) and on the initial mass of the core have been expressed. A 10% increase on the standard value of the energy density flux on the shock wave front in region I is indicated by $\epsilon_I + 10\%$ (col. [4]). Variations to the other parameters are sketched on this first row in a similar way.

© American Astronomical Society • Provided by the NASA Astrophysics Data System

1990ApJ...364..212H

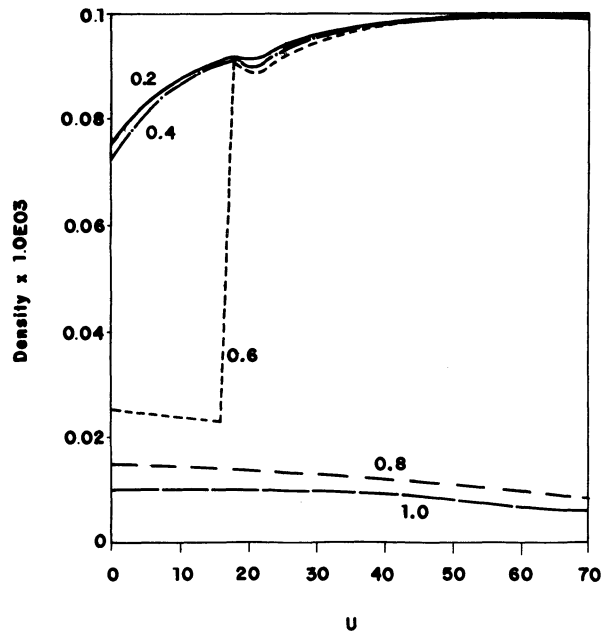

FIG. 3*a*

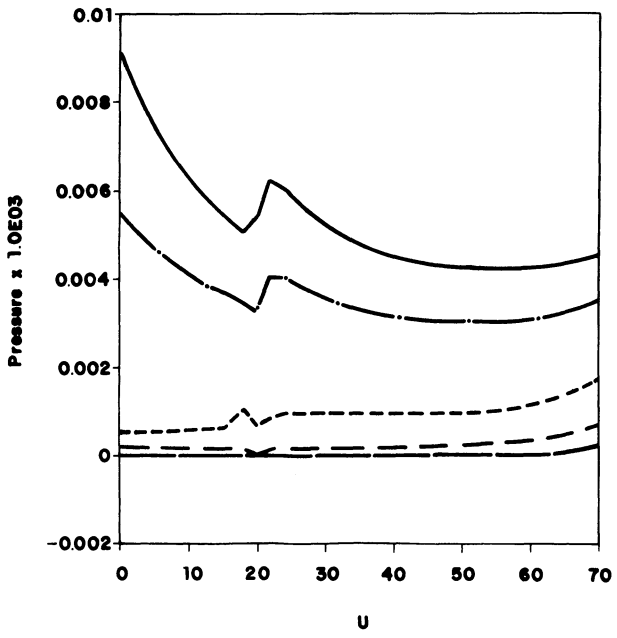

FIG. 3*b*

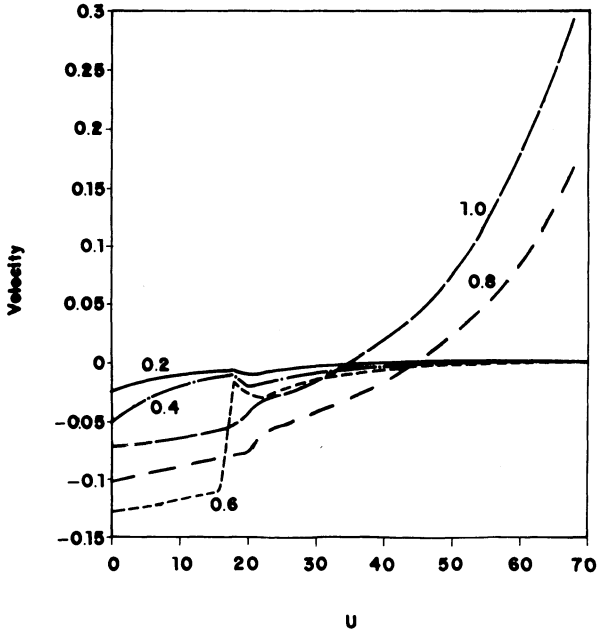

FIG. 3*c*

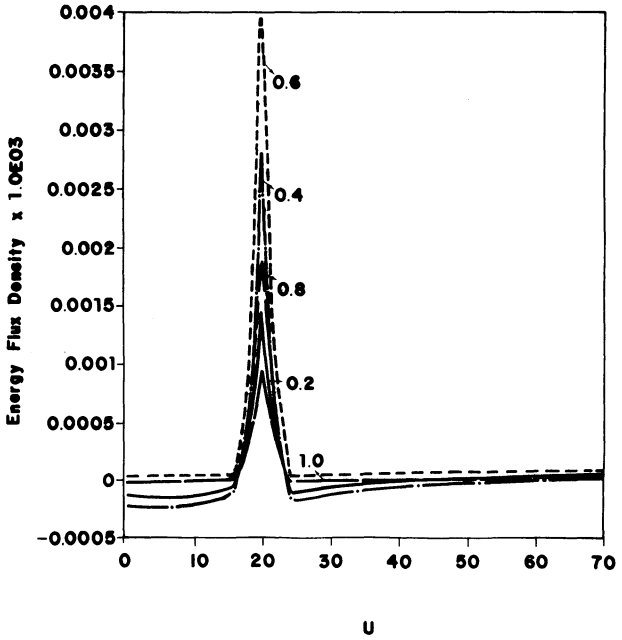

FIG. 3*d*

FIG. 3.—Evolution of the physical variables. (*a*) Density, (*b*) pressure, (*c*) mass velocity, and (*d*) energy flux density are monitored at five different fixed-mass shells. Curves are labeled by the corresponding ratios $r/a_0 = 0.2, 0.4, 0.6, 0.8, 1.0$.

In the first column (labeled "0"), there are 10 combinations of different profiles at the surface of the sphere and at both sides of the shock. The one-pulse shape has PW1 = 1.2 and TFP = 20.0 or 30.0, and the two-pulse profile has PW1 = 1.2, PW2 = 1.2, TFP = 25.0, STP = 10.0, and PHR = 1.0. The other parameters retain their standard values.

IV. DISCUSSION OF THE RESULTS

Before discussing the results themselves, we would like to emphasize the most important features which establish this scheme as a consistent and workable framework in general-relativistic radiating hydrodynamics.

The matter distribution considered is free of singularities everywhere. Rankine-Hugoniot relations match, through the shock, the inner and the outer solutions. The junction conditions across the boundary surface satisfy the remaining coupling with the radiating

© American Astronomical Society • Provided by the NASA Astrophysics Data System

1990ApJ...364..212H

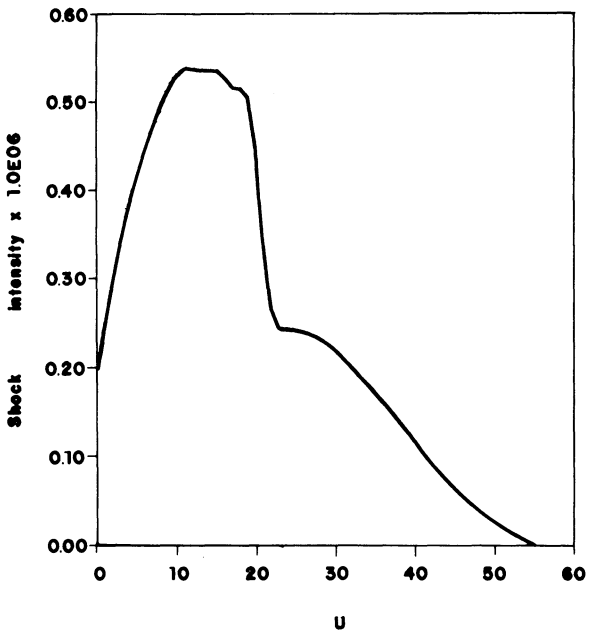

FIG. 4.—Time evolution of the intensity of the shock, $\mathcal{I} = P_{II} - P_I$

versions of the Schwarzschild exterior solution (the Vaidya solution). A heuristic assumption relating pressure, energy density, and the radial velocity of matter leads (via the junction conditions at the boundary and the Rankine-Hugoniot relations) to a system of ordinary differential equations for quantities evaluated at either the boundary surface or the shock front. This *Ansatz*, chosen on a solid physical ground, relates the equation of state in the inner core to the generalization of the Schwarzschild homogeneous interior solution, considered to be a stiff equation of state for ultradense matter, because it describes an incompressible fluid in the static limit. For the outer mantle the equation of state is inspired in the Tolman VI static solution which represents a highly relativistic Fermi gas.

TABLE 1

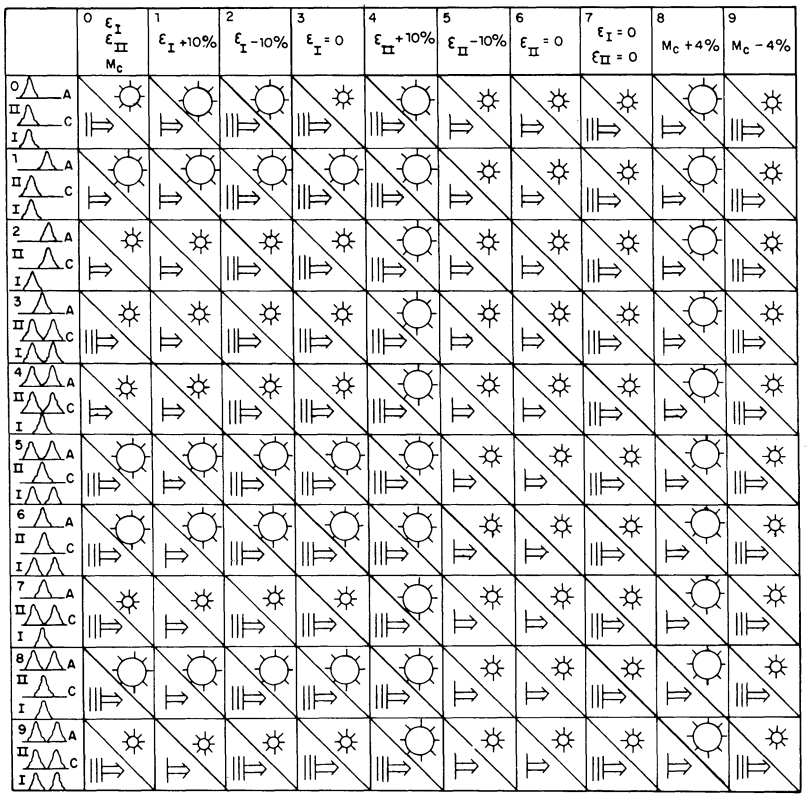

© American Astronomical Society • Provided by the NASA Astrophysics Data System

1990ApJ...364..212H

Notice that the general form of the energy-momentum tensor used to describe the fluid in both regions,

$$T_{\mu\nu} = (\rho + P)U_\mu U_\nu - Pg_{\mu\nu} + \epsilon K_\mu K_\nu ,$$

constrains radiation to travel radially along the null vector

$$K_\mu = (1 - 2\tilde{m}/r)^{1/2}\delta^1{}_\mu ,$$

i.e., the free-streaming limit approximation is assumed throughout the sphere except on the boundary and at both sides of the shock front. On these surfaces it is possible to shape at will the profiles of the radiation flux density and to introduce delays in time for the emission and absorption of the radiation pulse. This assumption makes it feasible to study radiation-hydrodynamic scenarios through the sphere, and not be restricted to only the free-streaming approximation. Table 1 summarizes the influence of particular combinations of different pulse shapes on the bouncing of the sphere and on the strength of the shock. But before discussing these results, the evolution of the standard model defined has to be considered.

Since the timelike coordinate is also a scaled variable, the characteristic times for the hydrodynamic processes discussed below may be associated to the radiation time scale, which is related to the width of the radiation pulse itself.

In Figure 2 the evolution of both the radius of the sphere (the boundary surface) and the shock wave front is sketched. As can be appreciated from this figure, the position of the shock remains almost constant, although the boundary surface bounces. Figures 3*a*–3*d* displays the profiles for energy density, pressure, the radial velocity, and radiation flux density, respectively. It is apparent from Figure 3*c* that the outermatter shells bounce earlier than inner ones. This bouncing scheme is maintained until the shock surface is reached. Moreover, during the bounce of the mantle, the shock wave separating the compact inner core from the outer mantle fades out (Fig. 4). Therefore, the early discontinuity surface bounding the core evolves into a boundary of the static and homogeneous remnant. As mentioned in § I, the origin of the peculiar bouncing of the mantle is to be found in the assumption of a free streaming-out radiation field propagating outward through the outer mantle with a Tolman VI–like equation of state. In fact, Herrera, Jiménez, and Ruggeri (1980) originally found this scheme of bouncing for a Tolman VI–like sphere, assuming as well a free streaming-out radiation field. Recent calculations (Barreto, Herrera, and Santos 1989) for the same Tolman VI model but in the diffusion limit approximation yield the opposite picture for the bouncing; i.e., inner shells bounce earlier than the outer ones.

a) Pulse-Shape Independent Parameters

Conclusions from Table 1 can be classified as pulse shape independent parameters. Columns (4)–(7) contain the influence of the total energy flux density on the shock at the mantle. Columns (8) and (9) enclose the relevance of the mass of the core. Both quantities emerge as decisive parameters affecting the bounce of the sphere. The more energy the shock deposits on the mantle, or the more massive the core is (within the values considered here), the stronger the bounce results.

As expected, the mean intensity of the shock is related to the radiation flux discontinuity across the shock:

$$\|\Rightarrow \quad \text{strong shocks} \quad \Leftrightarrow \quad [\epsilon] \geq 0 ,$$

$$|\Rightarrow \quad \text{weaker shocks} \quad \Leftrightarrow \quad [\epsilon] < 0 .$$

This result is related to the contribution of the radiation pressure discontinuity $[\epsilon]$ to the mean intensity of the shock $\bar{\mathcal{I}}_{ij}$.

b) The Changing Radiation Pulse

Columns (0)–(3) enclose the effect of a change of the pulse shape at the shock front, at the boundary surface, or on both the sphere bouncing and the shock strength. This influence has been observed when we considered standard values for the mass of the inner core and for the total radiation flux energy density at both sides of the shock front (col, [0]) and when the total radiation flux energy density at the shock front on the core side have been varied (cols. [1]–[3]). The modifications of the radiation pulse shape denote departures from the free-streaming approximations and may represent complex radiation transfer phenomena through the sphere.

Differing from the constant shock opacity parameter of our previous work (Herrera and Núñez 1987), $E_{\rm I} = \alpha E_{\rm II}$, situations where a time-dependent transfer function changes the pulse shape are sketched in rows 2, 4, 5, 6, and 7. In particular, rows 4 and 5 (and equivalently, 6 and 7) suggest that a *concentration* of two pulses into one leads to stronger explosions than the inverse combination of pulse shapes across the shock. The opposite picture is obtained when this phenomenon is simulated on the boundary surface (rows 3 and 8).

The effect of a *pulse delay* on the boundary surface and on the shock front are enclosed in rows 1 and 2. As can be seen from these rows, stronger bounces are associated to *pulse delays* on the surface, and fainter ones correspond to delays on the shock front.

It is apparent from Table 1 that the shock does not appear to be directly responsible for the expulsion of the outer envelopes of the sphere material, but it is closely related to it. It is also well-established that a deeper recession of the shock front is related to a stronger explosive ejection. This peculiar recession-explosion association and the general hydrodynamic scenario obtained recall those situations where the long-term mechanism leads to viable supernova outcomes. However, we do not find any revival of the original shock. Should the picture above turn out to be a suitable description of a supernova event, then strong shock fronts will no longer be required to explain the ejection of the outer envelope, nor will it be necessary to look for the revitalization of stalled shocks. Moreover, the surface which delimits the remnant is the shock itself once it has faded out and has been transformed into a boundary. If the interface propagates outward, the inner core grows by accretion of the outer mantle onto it, which would hinder stabilization of the appropriate ejection conditions.

Above, we have tried to exhibit the intrinsic relation between the "optical" properties of a detected burst and the corresponding hydrodynamic scenario of the source. However, to accomplish this task we have been forced by our own limitations to adopt some rather strong assumptions concerning the choice of the equation of state for both the inner core and the outer mantle. Although our

© American Astronomical Society • Provided by the NASA Astrophysics Data System

1990ApJ...364..212H

selection is not completely deprived of physical meaning, it is clear that a choice based on a more realistic treatment for the ultradense matter would lead to results more appealing to people working on supernova explosions.

In this regard, we are aware that there is a missing link between the specific luminosity profile and the particular regime of radiation transport, on one hand, and the description of the corresponding underlying microphysics, on the other. In this sense we consider this work not to be a definitive, self-contained model for a supernova explosion but rather a proposition for further participative research.

The erratum in Herrera and Núñez (1987), which we have pointed at in the appendix of the present work corresponding to the equation defining τ_4, leads to a different conclusion when the influence of the relativistic deviation of the core is examined. More massive cores deliver more violent explosion. The other results remain valid and seem to be independent of the particular pulse combination (neutrino transfer scene) considered.

One of us (L. H) gratefully acknowledges the financial support from the Fundación Polar and Dirección Nacional de Investigación Científico Técnica de España (D.E.I.C.y T. Spain). L. A. N. would like to thank Professor M. Abramowicz for the hospitality at the Astrophysics Group of the International Centre for Theoretical Physics, in Trieste, Italy. We would also like to thank the Centro Científico IBM de Venezuela (IBM Scientific Center of Venezuela) where part of the computational work was carried out, especially to C. Mendoza and J. Rivero for their helpful advice. This work has been partially supported by the Consejo de Desarrollo Científico y Technológico de la Universidad de Los Andes Mérida-Venezuela (CDCHT-ULA), under project 379-89-05.

APPENDIX

In Appendix II of Herrera and Núñez (1987), the generalized Tolman-Oppenheimer-Volkoff equation is

$$\dot{\Omega} = \tau_1 \frac{\dot{F}}{F} + \tau_2 \frac{\dot{C}}{C} + \tau_3 \frac{\dot{G}}{G} + \tau_4 ,$$

and the corresponding coefficients should read

$$\tau_1 = 1 + \frac{AF}{A(1-F) - C(1-G)}, \qquad \tau_2 = \frac{AC(F-G)}{(A-C)A(1-F) - C(1-G)}, \qquad \tau_3 = -\frac{AG}{A(1-F) - C(1-G)},$$

$$\tau_4 = \frac{(\Omega - 1)}{2A\Omega}\left[24\pi H(3\Omega - 1) - \Omega(F+3) - 4F\Omega^2\right] + \frac{1}{8A}\left\{-3F + 4(1-F)\left[\Omega - \frac{24\pi H(\Omega - 1)}{(1-F)}\right]\right\} + \frac{F(\Omega - 1)}{A}\left[2 - \frac{AC(F-G)}{(A-C)A(1-F) - C(1-G)}\right].$$

Notice the minus sign in the last term of τ_4, differing from the one that appeared in Herrera and Núñez (1987).

REFERENCES

Aglietta, M., *et al.* 1987, *Europhys. Letters*, **3**, 1315.
Arnett, W. D. 1987, *Ap. J.*, **319**, 136.
Baron, E., Bethe, H. A., Brown, G. E., Cooperstein, J., and Kahana, S. H. 1987, *Phys. Rev. Letters*, **59**, 736.
Barreto, W., Herrera, L., and Santos, N. O. 1989, *Ap. J.*, **344**, 158.
Bionta, R. M., *et al.* 1987, *Phys. Rev. Letters*, **58**, 1494.
Bondi, H. 1964, *Proc. Roy. Soc. London A*, **281**, 39.
Bruenn, S. W. 1987, *Phys. Rev. Letters*, **59**, 938.
De Rújula, A. 1987, *Phys. Letters*, **193B**, 514.
Herrera, L., Jiménez, J., and Ruggeri, G. 1980, *Phys. Rev. D*, **22**, 2305.
Herrera, L., and Núñez, L. 1987, *Ap. J.*, **319**, 868.
Hillebrandt, W., Höflich, P., Kafka, P., Schimidt, H. U., and Truran J. W. 1987, *Astr. Ap.*, **180**, L20.
Hirata, K., *et al.* 1987, *Phys. Rev. Letters*, **58**, 1490.
Kahana, S. H., Cooperstein, J., and Baron, E. 1987, *Phys. Letters*, **196B**, 256.
Lattimer, J. M. 1988, *Nucl. Phys. A*, **478**, 119c.
Sawyer, R. F. 1988, *Ap. J.*, **328**, 691.
Stella, A., and Treves, A. 1987, *Astr. Ap.*, **185**, L5.
Taub, A. H. 1948, *Phys. Rev.*, **74**, 328.
———. 1983, in *Proc. 3d Marcel Grossman Meeting on General Relativity*, ed. H. Ning (Amsterdam: Science Press and North Holland), p. 165.
Tolman, R. C. 1939, *Phys. Rev.*, **55**, 364.

LUIS HERRERA: Apartado 80793, Caracas 1080A, Venezuela

LUIS NÚÑEZ: Apartado 54, Mérida 5101A, Venezuela

© American Astronomical Society • Provided by the NASA Astrophysics Data System